SCIENTIFIC REPORTS

OPEN

SUBJECT AREAS:
PHASE TRANSITIONS AND CRITICAL PHENOMENA
LASER-PRODUCED PLASMAS
MATERIALS FOR OPTICS

Received
16 October 2013

Accepted
20 March 2014

Published
8 April 2014

Correspondence and requests for materials should be addressed to Z.L.L. (zlli@jlu.edu.cn) or C.L.S. (chenglin@jlu.edu.cn)

Raman spectra from Symmetric Hydrogen Bonds in Water by High-intensity Laser-induced Breakdown

Zhiwei Men[1,2], Wenhui Fang[2], Dongfei Li[2], Zhanlong Li[2] & Chenglin Sun[1]

[1]State Key Laboratory of Superhard Materials, Jilin University, Changchun 130012, China, [2]College of Physics, Jilin University, Changchun 130012, China.

Raman spectra of ice VII and X were investigated using strong plasma shockwave generated by laser-induced breakdown (LIB) in liquid water. Simultaneously, the occurrence of the hydrogen emission lines of 656 nm (Hα), 486 nm (Hβ), 434 nm (Hγ) and 410 nm (Hδ) was observed. At 5×10^{12} W/cm^2 optical power density, the O-H symmetric stretching, translational and librational modes of ice VII and a single peak at 785 cm^{-1} appeared in the spectra. The band was assigned to the Raman-active O-O mode of the monomolecular phase, which was the symmetric hydrogen bond of cuprite ice X. The spectra indicated that ice VII and X structure were formed, as the trajectory of the strong plasma shockwave passes through the stable Pressure-Temperature range of ice VII and X. The shockwave temperature and pressure were calculated by the Grüneisen model.

The behavior of water at conditions of extreme pressure and temperature is of profound importance to planetary science, geoscience, and fundamental chemistry[1]. Of particular interest has been the pressure-induced transformation to nonmolecular forms, a transition connected with hydrogen-bond symmetrization[2]. Ice X, the symmetric ice structure, was detected at 44 GPa in a diamond-anvil cell by Brillouin scattering[3]. Infrared (IR) measurements have provided evidence for the transition from ice VII (or ice VIII at lower temperature[4]) to a phase with symmetric hydrogen bonds-ice X beginning at around 60 GPa and stable to at least 210 GPa[5–7]. The melting curve showed a discontinuous change in slope at about 43 (47) GPa and 1600 (1000) K using Raman spectra, indicating a phase transition most likely from the ice VII to the ice X phase[8,9].

Until recently, the experimental study of water phase transition at extreme conditions was limited mainly to use a laser heated the static diamond anvil cell. Holmes et al. obtained a spontaneous Raman scattering from shocked water, the strong shockwaves were generated by planar impactors accelerated to 2.1–3.2 km/s by a two-stage light-gas gun[10].We performed the experiments using a high-intensity laser-induced shockwave compression to obtain high-temperature and dynamic high-pressure[11,12]. LIB refers to plasma production carried out by focusing an intense pulsed laser beam in substances. When the laser pulse duration is longer than a few nanoseconds, plasma cloud evolves by directly absorbing the laser power. The rapid expansion in the ionization region creates an intense shock wave coming out from the plasma cloud and propagating in the medium at supersonic speed. The plasma region is composed of a central low refractive index distribution with $n < 1$ and a spherical high-density distribution whose distance is increasing from the origin of the shockwave expansion[13]. Currently, the long-range order ice VIII (H_2O) and the short-range order ice VII (D_2O) have been obtained by LIB[11,12].

In this letter, an experimental study has been carried out on the dynamical process taking place in the strong plasma shockwave generated by an intense 12 ns (FWHM) pulse beam focused into liquid water. The occurrence of the hydrogen emission lines of 656 nm ($H\alpha$), 486 nm ($H\beta$), 434 nm ($H\gamma$) and 410 nm ($H\delta$) was observed. At the same time, the Raman peaks of *O-H* stretching vibrational region, three low-frequency Raman Stokes peaks and their intense anti-Stokes peaks were obtained, which present: (1) The characteristic Raman spectrum that developed from the symmetric hydrogen bonds of ice X at 5×10^{12} W/cm^2 optical power density; (2) One internal-mode Raman spectrum that belongs to the *O-H* stretching vibration, one translational mode *T*, and one librational mode *R* of ice VII. These phenomena are attributed to the ice VII and X formation in liquid water induced by strong plasma shockwave.

Results

We attempted to determine the phase transition trajectory of ice by laser-induced strong plasma shockwave. We found that this method yields rich in atom and molecule spectra compared to the hydrostatic pressure.

Representative Raman spectra in liquid water under the different optical power density are shown in Fig. 1. The high-frequency *O-H* stretching vibrations in H_2O ice VII form a doublet, which has been assigned to $\nu_1(A_{1g})$ and $\nu_3(E_g)$ modes in order of increasing frequency (ice VII, point group of O_h^4)[14]. These modes are softening with pressure[15], the softening effect can be seen from Fig. 1(a, c), whose positions are corresponding with that of H_2O at the around 17 GPa and 33 Gpa pressure[14] respectively. The frequencies of all components of the *O-H* band increase with temperature indicating that the hydrogen bond in ice VII weakens as the melting transition is approached and molecules acquire larger translational disorder[9]. The hydrogen emission line of *Hα*-656 nm was also observed (Fig. 1 (a, c)).

Measurements in the low-frequency range reveal several important spectrum characteristics (Fig. 1 (b)). We find two special peaks in the spectrum at the same optical power density, a Stokes Raman line and its anti-Stokes Raman line, whose Raman shift are ± 785 cm^{-1} that characterizes the ice X cuprite structure[16], the mode display an increase in frequency as the pressure increased[17], which corresponding with the pressure should be at around 65 GPa[6]. A likely assignment in order of increasing frequency is $T_z(A_{1g}) + T_{xy}(E_g)$ and $T_z(B_{1g}) + T_{xy}(E_g)$ that are unresolved bands for the translational bands at the around 370 cm^{-1}, $R_{xy}(E_g) + R_z(E_{2g})$ for the librational bands at around 605 cm^{-1}, the Raman shift corresponding with pressure should be approximate 17 GPa[14]. In Fig. 1 (d), these two Raman shifts are around 360 and 595 cm^{-1} respectively, which display an increase in frequency as the pressure increased. Another spectrum characteristic is that the intensity of anti-Stokes peak is similar to that of Stokes peak.

Discussion

The Carnegie group succeeded in determining the VII-X transformation zone in 1999, this transformation was characterized by the disappearance of the $T_z(A_{1g}) + T_{xy}(E_g)$ and $T_z(B_{1g}) + T_{xy}(E_g)$ (where the two peaks were not resolved) lattice modes of ice VII, and progressive occurrence of the expected Raman-active F_{2g} mode[17]. The lower pressure limit of the transformation was found close to the isobar 62 GPa[18].

In this experiment, the Raman spectra of ice VII and X can be obtained, because high-intensity LIB generate the strong plasma shockwave, which make a dynamic high-pressure and high-temperature field around the focal point. The mechanism of ice formation using LIB has been discussed by our group[11]. A 1×10^{12} W/cm^2

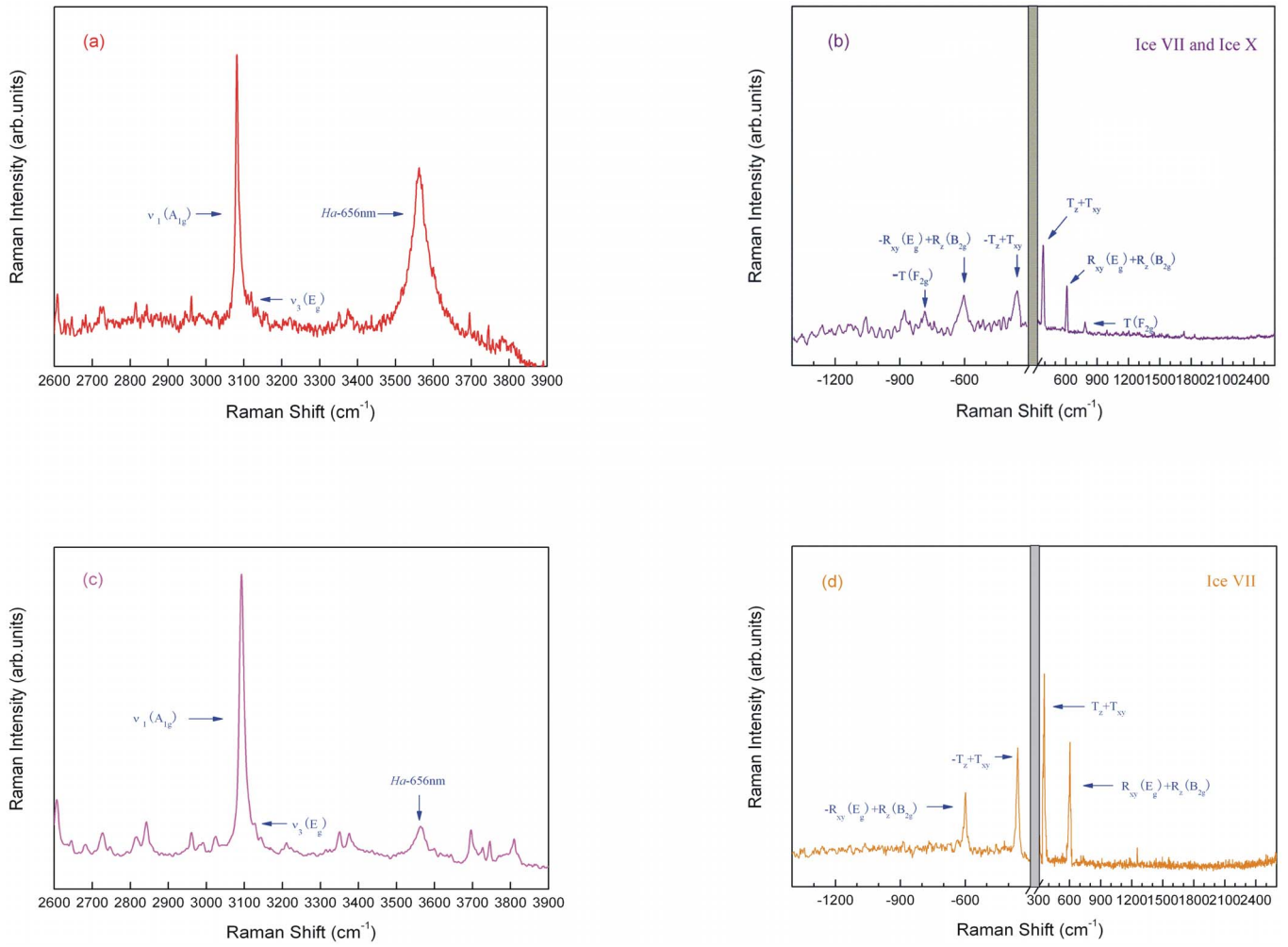

Figure 1 | Representative Raman spectra of ice VII and ice X by LIB. (a) The spectrum of *O-H* stretch vibration (~3080 cm^{-1}) in ice VII and *Hα* (656 nm) line. (b) The unresolved $T_z + T_{xy}$ ($T_z(A_{1g}) + T_{xy}(E_g)$ and $T_z(B_{1g}) + T_{xy}(E_g)$) bands around 370 cm^{-1} and $R_{xy}(E_g) + R_z(B_{2g})$ bands around 605 cm^{-1} belong to the translational and librational modes of the ice VII respectively. The $T(F_{2g})$ peak, which characterizes the ice X cuprite structure, is around 785 cm^{-1} in ice X. (c) The spectrum of *O-H* stretch vibration (~3070 cm^{-1}) in ice VII and *Hα* (656 nm) line.(d) The unresolved $T_z + T_{xy}$ ($T_z(A_{1g}) + T_{xy}(E_g)$ and $T_z(B_{1g}) + T_{xy}(E_g)$) bands around 360 cm^{-1} and $R_{xy}(E_g) + R_z(B_{2g})$ bands around 595 cm^{-1} belong to the translational and librational modes of the ice VII respectively. The rectangle centered at zero frequency mask peculiarity associated with the subtraction of elastically scattered radiation. The optical power density of Fig. 1 (a, b) is 5×10^{12} W/cm^2, and that of Fig. 1 (c, d) is 2×10^{12} W/cm^2.

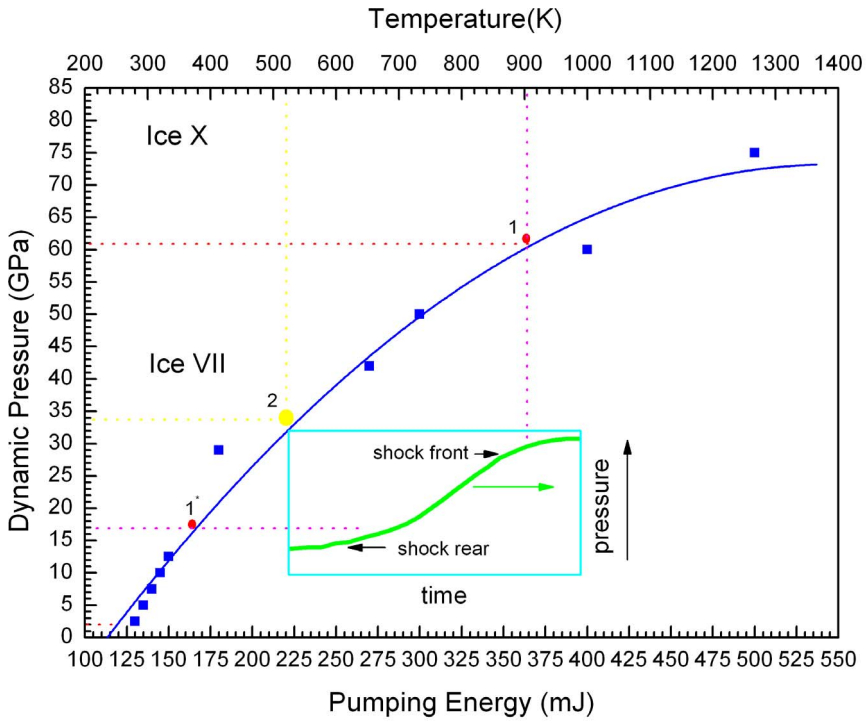

Figure 2 | Dynamic pressure-temperature phase diagram of ice in the region VII-X. Blue closes squares, dynamic pressure at different pumping energy for H_2O, corresponding blue solid lines. Horizontal doted lines at ~2 GPa and ~62 Gpa, expected liquid-VII and VII-X transition lines for H_2O respectively. Insert: A shockwave front moving through a medium, the shockwave pulse falls more slowly than it rises[19]. A magenta horizontal and a magenta vertical dot lines are corresponding with the dynamic pressure and temperature of one shock rear and front at pumping energy around 500 mJ, which corresponds to Fig. 1(a, b). A yellow horizontal and a yellow vertical dot lines are corresponding with the dynamic pressure and temperature of the yellow closed circle 2 at pumping energy around 275 mJ, which corresponds to Fig. 1(c, d). These closed circles are from the experimental data.

optical power density is enough to induce breakdown of pure water and some organic solvents[20,21]. First, the rising edge of the laser pulse whose duration is about 12 ns interacts with water, and LIB is generated when the pulse peak arrives at the focal point. Simultaneously, the plasma bubble that has a diameter of hundreds of microns is also obtained[20,22]; Second, the plasma bubble begins to collapse and produces strong shockwave that induce water compression, the shockwave speed and the particle velocity is approximate 8.4 and 2.4 km/s, respectively[20,23]. The strong plasma shockwave front rises faster in water, whose duration is around 10 ns, and its pulse falls whose duration is around 100 ns more slowly than it rises. Ice X can be formed when the shockwave front rises, the temperature is around 900 K and the pressure is around 65 Gpa[19,23,24], which corresponding with the experimental result point 1 in Fig. 2. The water pressure declines slowly and uniformly[19]. The shockwave generates approximately 17 Gpa pressure and 350 K temperature[23–30] when the shock wave pulse falls (Point 1* in Fig. 2). Under these conditions, ice VII can be obtained[14]. We estimated temperature by analyzing the relative intensities of the Stokes and anti-Stokes peaks according to the equation $T = \frac{hc\upsilon_k}{K} \Big/ \left[\ln\frac{I_s}{I_a} + 4\ln\left(\frac{\upsilon_0+\upsilon_k}{\upsilon_0-\upsilon_k}\right)\right]$[31]. The intensities of Stokes and anti-Stokes lines depend on the population of the particles of the correlated ground and excited state of the specific vibrations. The Stokes-to-anti-Stokes intensity technique was adopted because it

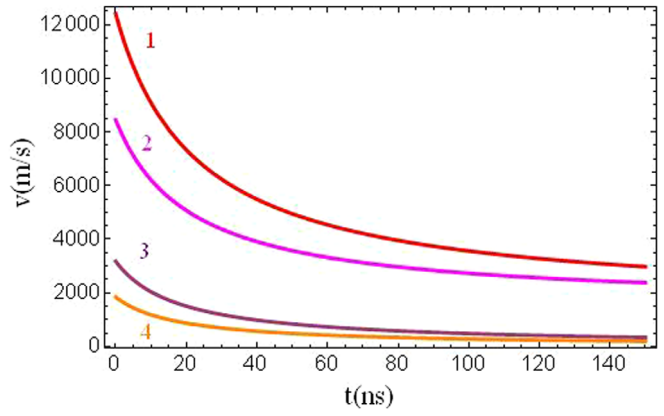

Figure 3 | Experimentally determined shockwave velocity v_s and particle velocity v_p behind the shockwave front plotted as a function of the time delay between laser pulse and illumination pulse. Curve 1 and 3 show the shockwave velocity and the particle velocity at pumping energy around 500 mJ, respectively. Curve 2 and 4 show that at pumping energy around 275 mJ, respectively.

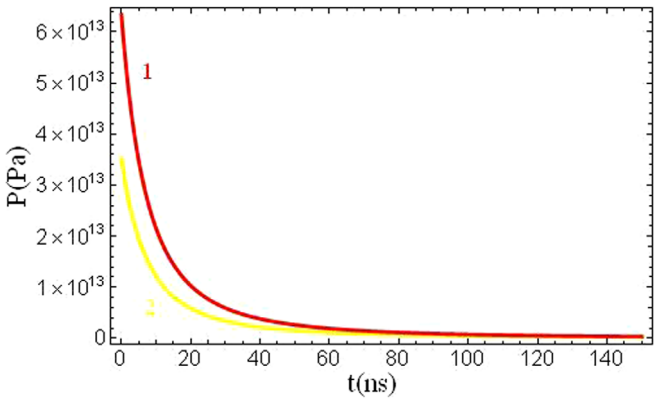

Figure 4 | Shockwave pressures of the numerical calculations for pumping energy with 500 mJ (curve 1) and 275 mJ (curve 2).

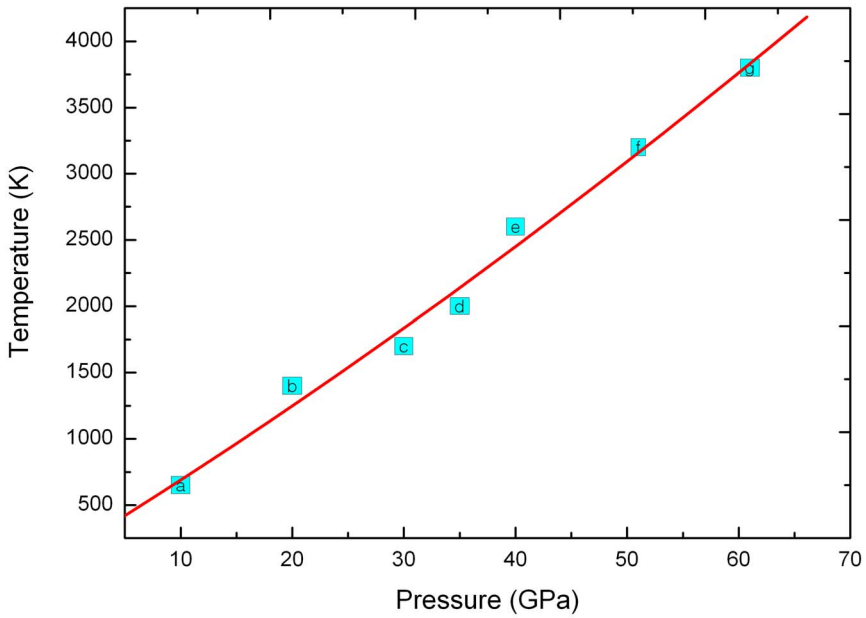

Figure 5 | Shockwave temperature data plotted as a function of pressure. Points a and b taken to $C_v = 7.1R$, and points c, d, e, f and g taken to $C_v = 8.7R$.

is based on an intrinsic property of the studied system. The Raman peaks of ice X show a higher temperature than that of ice VII based on the equation. Third, the descending edge whose duration is approximate 12 ns of the laser pulse excites ice VII and X, and the Raman spectra of ice VII and X are observed. Two reasons affirm that the Raman spectra belong to ice VII and X. (1) The lattice translation of 370 cm^{-1} at low frequency is the characteristic peak of ice VII, and the disappearance of the translational peak 370 cm^{-1} of ice VII is interpreted as a transition into ice X. (2) the Raman-active F_{2g} mode of 785 cm^{-1} characterizes the ice X cuprite structure, only the symmetric hydrogen bonds can generate this Raman band in ice[16].

The shockwave pressure and temperature were calculated as the following.

According to the plasma particle velocity $v_p(t)$ that was obtained by fluorescence imaging techniques, and the relationship between v_p and v_s[32],

$$v_p = c_1(10^{(v_s - c_0)/c_2} - 1) \quad (1)$$

v_s is the shockwave velocity, the curves of shockwave and particle velocity were drew in Fig. 3. Base on the v_s values, the shockwave pressure $p_s(t)$ can be also calculated using the equation,

$$p_s = c_1\rho_0 v_s(10^{(v_s - c_0)/c_2} - 1) + p_\infty \quad (2)$$

$p_s(t)$ curves are drew in Fig. 4. According to it, the shockwave front rises faster, and its pulse falls more slowly than it rises.

We put to use the Grüneisen model to calculate the shockwave temperature[33].

$$\gamma = V(\frac{\partial P}{\partial E})_V \quad (3)$$

If at a given volume, the Hugoniot pressure P_H is known as well as the state (P_r, T_r), then Eq.(3) allows evaluation of the internal energy difference between these states. In this case,

$$E_H - E_r = \int_{P_r}^{P_H} \frac{V}{\gamma} dP = \int_{T_r}^{T_H} C_v(V,T)dT \quad (4)$$

When, at any given V, the appropriate value of γ is assumed independent of temperature, then $P_\gamma = P_s(V)$ can be calculated numerically, which in turn leads to the solution of Eq.(4) for the theoretical shockwave temperature T_H. In the present case, temperature calculations using a constant $\gamma = 0.9$[34]. The specific heat C_v has a much greater effect in shockwave temperature calculations. The value of $C_v = 7.1R$ and $C_v = 8.7R$ per mol of H_2O was used for low and high pressure, respectively. R is ideal gas constant.

Fig. 5 shows the measured shockwave temperatures plotted as a function of principal Hugoniot pressure. The temperature is higher than that previously calculated by Stokes-to-anti-Stokes intensity technique, because of two reasons. (1) Water temperature drops quickly[23], when there are a large number of water molecules surrounding shockwave front at room temperature. (2) Shockwave can lead water volume V to largening rather than a constant, so the Hugoniot temperature is higher than actual temperature.

In conclusion, we have observed the hydrogen emission spectra and Raman spectra of ice VII and X when LIB is generated in liquid water. The LIB generates a high-temperature and dynamic high-pressure field, which lead to the intensity of anti-Stokes be close to that of Stokes. Ice VII and X were formed by the strong plasma shockwave rear and front respectively. The shockwave pressure and temperature are calculated by the Grüneisen model. The study confirmed that ice X transforms from ice VII under the dynamic pressure condition. Last but not least we have developed a powerful tool to study on the phase transition of liquid system.

Methods

Raman scattering experiments of water. A frequency-doubled Nd:YAG laser is used as the excitation laser for laser-induced breakdown of liquid water, which emitted laser pulse duration of 12 ns with a wavelength of 532 nm. It has a repetition rate of 1 Hz and pulse energy in the range of 0–700 mJ. The laser is coupled to a 10 cm-long quartz cell with 25 times magnification object lens. The output light is focused on the AvaSpec-2048-5-USB2 fiber optic spectrometers, whose spectral resolution is 0.05 nm, and the signals are managed by a computer. The experimental setup is shown elsewhere[24].

Fluorescence imaging experiments. The plasma fluorescence imaging of water is obtained by the PI- Max ICCD, whose image resolution is 1024 × 1024, the shutter duration is 2 ns. The interval time of sampling is 2 ns. A 656 nm filter is used to achieving the around 656 nm wavelength fluorescence imaging for obtaining the particle velocity.

Computation. In our studies, calculations of shockwave pressure and temperature are performed by using the Mathematica soft.

1. Knudson, M. D., Desjarlais, M. P. & Dolan, D. H. Shock-wave exploration of the high-pressure phases of carbon. *Science.* **322**, 1822–1825 (2008).

2. Lee, C., Vanderbilt, D., Laasonen, K., Car, R. & Parrinello, M. Ab initio studies on high pressure phases of ice. *Phys. Rev. Lett.* **69**, 462–465 (1992).
3. Polian, A. & Grimsditch, M. New high-pressure phase of H_2O: Ice X. *Phys. Rev. Lett.* **52**, 1312–1314 (1984).
4. Song, M., Yamawaki, H., Fujihisa, H., Sakashita, M. & Aoki, K. Infrared investigation on ice VIII and the phase diagram of dense ices. *Phys. Rev. B.* **68**, 014106 (2003).
5. Goncharov, A. F., Struzhkin, V. V., Somayazulu, M., Hemley, R. J. & Mao, H. K. Compression of ice to 210 GPa: evidence for a symmetric hydrogen bonded phase. *Science.* **273**, 218–220 (1996).
6. Aoki, K., Yamawaki, H., Sakashita, M. & Fujihisa, H. Infrared absorption study of the hydrogen-bond symmetrization in ice to 110 GPa. *Phys. Rev. B.* **54**, 15673–15677 (1996).
7. Struzhkin, V. V., Goncharov, A. F., Hemley, R. J. & Mao, H. K. Cascading Fermi resonances and the soft mode in dense ice. *Phys. Rev. Lett.* **78**, 4446–4449 (1997).
8. Schwager, B., Chudinovskikh, L., Gavriliuk, A. & Boehler, R. Melting curve of H_2O to 90 GPa measured in a laser-heated diamond cell. *J. Phys.: Condens. Matter.* **16**, S1177–S1179 (2004).
9. Goncharov, A. F. *et al.* Dynamic ionization of water under extreme conditions. *Phys. Rev. Lett.* **94**, 125508 (2005).
10. Holmes, N. C., Nellis, W. J., Graham, W. B. & Walrafen, G. E. Spontaneous Raman scattering from shocked water. *Phys. Rev. Lett.* **55**, 2433–2436 (1985).
11. Men, Z. W. *et al.* Stimulated Raman scattering from ice-VIII by shock-induced compression in liquid water. *Phys. Rev. B.* **85**, 092101 (2012).
12. Li, Z. L. *et al.* Stimulated Raman scattering of lattice translational modes in liquid heavy water. *Opt. Lett.* **37**, 1319–1321 (2012).
13. Siano, S., Pini, R., Salimbeni, R. & Vannini, M. A diagnostic set-up for time-resolved imaging of laser-induced ablation. *Opt. Las. Eng.* **25**, 1–12 (1996).
14. Pruzan, Ph., Chervin, J. C. & Gauthier, M. Raman spectroscopy investigation of Ice VII and deuterated ice VII to 40 GPa. disorder in ice VII. *Europhys. Lett.* **13**, 81–83 (1990).
15. Pruzan, Ph., Chervin, J. C. & Canny, B. Determination of the D_2O ice VII–VIII transition line by Raman scattering up to 51 GPa. *J. Chem. Phys.* **97**, 718–721 (1992).
16. Putrino, A. & Parrinello, M. Anharmonic Raman spectra in high-pressure ice from Ab Initio simulations. *Phys. Rev. Lett.* **88**, 176401 (2002).
17. Goncharov, A. F., Struzhkin, V. V., Mao, H.-K. & Hemley, R. J. Raman spectroscopy of dense H_2O and the transition to symmetric hydrogen bonds. *Phys. Rev. Lett.* **83**, 1998–2001 (1999).
18. Pruzan, Ph. *et al.* Phase diagram of ice in the VII–VIII–X domain. Vibrational and structural data for strongly compressed ice VIII. *J. Raman. Spectrosc.* **34**, 591–610 (2003).
19. Dlott, D. D. Nanoshocks in molecular materials. *Acc. Chem. Res.* **33**, 37–45 (2000).
20. Vogel, A., Busch, S. & Parlitz, U. Shock wave emission and cavitation bubble generation by picosecond and nanosecond optical breakdown in water. *J. Acoust. Soc. Am.* **100**, 148–165 (1996).
21. Cremers, D. A., Radziemski, L. J. & Loree, T. R. Spectrochemical analysis of liquids using the laser spark. *Appl. Spectrosc.* **38**, 721–929 (1984).
22. Yui, H., Fujiwara, H. & Sawada, T. Spectroscopic analysis of total-internal-reflection stimulated Raman scattering from the air/water interface under the strong focusing condition. *Chem. Phys. Lett.* **360**, 53–58 (2002).
23. Fedotov-Gefen, A. *et al.* Generation of a 400 GPa pressure in water using converging strong shock waves. *Phys. Plasmas.* **18**, 062701 (2011).
24. Li, Z. L. *et al.* Estimating the pressure of laser-induced plasma shockwave by stimulated Raman shift of lattice translational modes. *Appl. Phys. Lett.* **101**, 021908 (2012).
25. Vedadi, M. *et al.* Structure and dynamics of shock-induced nanobubble collapse in water. *Phys. Rev. Lett.* **105**, 014503 (2010).
26. Hendijanifard, M. & Willis, D. A. An improved method to experimentally determine temperature and pressure behind laser-induced shock waves at low Mach numbers. *J. Phys. D: Appl. Phys.* **44**, 145501 (2011).
27. Nath, A. & Khare, A. Effect of focusing conditions on laser-induced shock waves at titanium–water interface. *Appl. Opt.* **50**, 3275–3281 (2011).
28. Dolan, D. H., Knudson, M. D., Hall, C. A. & Deeney, C. Ametastable limit for compressed liquid water. *Nat. Phys.* **3**, 339–341 (2007).
29. Abramczyk, H. & Brozek, B. Is there a correlation between phase transition of phenylacetylene in liquids and frozen matrices and vibrational dynamics? *Chem. Phys.* **250**, 145–154 (1999).
30. Abramczyk, H. Femtosecond primary events in bacteriorhodopsin and its retinal modified analogs: Revision of commonly accepted interpretation of electronic spectra of transient intermediates in the bacteriorhodopsin photocycle. *J. Chem. Phys.* **120**, 11120–11132 (2004).
31. Malyj, M. & Griffiths, J. E. Stokes/Anti-Stokes Raman vibrational temperatures: reference materials, standard lamps, and spectrophotometric calibrations. *Appl. Spectrosc.* **37**, 315–333 (1983).
32. Rice, M. H. & Walsh, J. M. Equation of state of water to 250 kilobars. *J. Chem. Phys.* **26**, 824–830 (1957).
33. Lyzenga, G. A., Ahrens, Thomas, J., Nellis,W. J. & Mitchell, A. C. The temperature of shock-compressed water. *J. Chem. Phys.* **76**, 6282–6286 (1982).
34. Mitchell, A. C. & Nellis, W. J. Equation of state and electrical conductivity of water and ammonia shocked to the 100 GPa (1 Mbar) pressure range. *J. Chem. Phys.* **76**, 6273–6281 (1982).

Acknowledgments

This work is supported by the National Nature Science Foundation of China (No. 11104106), National Found for Fostering Talents of basic Science (No. J1103202), the Science and Technology Planning Project of Jilin Province (Nos. 201101037, 201201030, 20130101017JC, 20140101173JC, and 20140204077GX), and the China Postdoctoral Science Foundation (Nos. 2012M520669 and 2013M530973).

Author contributions

Z.W.M. conceived the project and wrote the final paper. W.H.F. wrote initial drafts of the work. Z.L.L. designed the experiments, synthesized and characterized the materials. D.F.L. and C.L.S. analyzed the Raman spectra. All authors discussed the results and commented on the manuscript.

Additional information

Competing financial interests: The authors declare no competing financial interests.

How to cite this article: Men, Z.W., Fang, W.H., Li, D.F., Li, Z.L. & Sun, C.L. Raman spectra from Symmetric Hydrogen Bonds in Water by High-intensity Laser-induced Breakdown. *Sci. Rep.* **4**, 4606; DOI:10.1038/srep04606 (2014).